Electrospun Carbon Nanofiber Webs with Controlled Density of States for Sensor Applications

Xianwen Mao, Fritz Simeon, Gregory C. Rutledge, and T. Alan Hatton**

Carbonaceous materials are of enormous interest, mainly due to their superior electrocatalytic activity for various chemical and biological systems.[1] The control of heterogeneous electron transfer kinetics through judicious design and structural manipulation of advanced carbon materials is of importance in the fabrication of many electrochemical devices such as biological sensors.[1c,2] Common strategies to accomplish this control include modification of surface chemistry,[1c] variation of graphene orientation,[3] and manipulation of surface roughness.[4] These strategies, however, offer little control over the density of electronic states (DOS) near the Fermi level, which plays a crucial role in the electrochemical activity of electrode materials.[1c,5] Lack of direct control of the intrinsic properties (i.e., DOS) of the electrodes results in an inability: 1) to modulate kinetics for outer-sphere systems because their kinetic behavior is only affected by the DOS of the electrode, and 2) to alter universally the kinetics for different types of inner-sphere systems since one particular strategy usually can only influence the kinetics of a specific inner-sphere system, not all of them. Also, the direct electron transfer (DET) with many redox enzymes strongly depends on the DOS of the supporting electrode.[6] Therefore development of an electrode with controlled DOS is necessary to modulate the DET efficiencies with enzymes for many applications such as highly selective biosensors,[7] bioelectronics,[8] enzyme catalysts,[9] and biofuel cells.[10]

Electrospinning is a simple and versatile technique to produce continuous nanofibers from various organic and inorganic materials.[11] Carbon nanofibers (CNFs) synthesized via electrospinning and subsequent carbonization have attracted attention mainly because their structures and properties can be easily adjusted by changing processing conditions.[12] The electrochemical applications of electrospun CNFs are mostly related to the development of energy storage devices including supercapacitors,[13] lithium-ion batteries,[14] and fuel cells.[15] Only a few reports focus on sensor applications of the electrospun CNFs, the electroanalytical activities of which are often adjusted through the use of an additional active component, such as loading or deposition of metal nanoparticles onto the fibers.[16]

In contrast, our work concentrates on manipulation of the intrinsic electronic properties of the electrospun CNFs for electrochemical sensing applications. We present a simple and highly effective strategy to adjust the electrochemical activities of electrospun CNF webs via controlling their DOS by processing conditions. Previous work in our group has shown that electrospun CNF webs from poly(vinylidene fluoride) or polyacrylonitrile can be used as free-standing and highly porous electrode materials with good electrochemical performances.[17] In this study we found that the use of electrospun CNF webs with adjustable DOS can modulate electron transfer kinetics and efficiencies for *various* chemical and biological systems. This further suggests that our strategy to control electron transfer processes can apply to different types of redox species, which is highly challenging since their electron transfer behaviors are usually affected by different factors.[1c]

The DOS of electrospun CNFs was controlled by selecting an appropriate polymer precursor (polyacrylonitrile, PAN) to generate nanosized graphite domains upon carbonization, and then varying the thermal treatment conditions to adjust the concentration of these graphite domains. Hereafter the CNF webs synthesized at carbonization temperatures of 1000, 1100, and 1200 °C are denoted as CNF1000, CNF1100, and CNF1200, respectively. When compared with large graphite domains, nanosized graphite domains with many edge-plane sites provide a significantly higher DOS near the Fermi level due to the overlap between the valence and conduction bands.[18] The concentration of nanometric graphite clusters in the CNF webs should have a significant impact on their DOS. Furthermore, these webs can be easily fabricated as free-standing electrodes without using binders or substrates, and electrospinning conditions can be fine-tuned to manipulate the surface area and porosity of the electrospun webs,[19] providing design flexibility such as improving immobilization of biomolecules. Therefore, electrospun CNF webs offer some distinct advantages for bioelectrocatalysis and electrochemical sensing over other carbon materials studied in molecular electrochemistry, such as nanostructured carbon films,[1c] CNTs,[2a] and graphenes.[2b]

Evidence of effective control over the graphite concentration and DOS of the CNF webs via varying carbonization conditions is presented in **Figure 1**. The porous CNF webs consist of fibers with diameters around 250 nm, which decrease slightly with increasing carbonization temperature (Supporting Information, Figure S1). X-ray photoelectron spectroscopy (XPS) C 1s spectra (Figure 1a) were used to quantify the sp^2/sp^3 ratio on the CNF surface and thus to estimate the graphite concentration (i.e., sp^2 carbon). Deconvolutions of the C 1s spectra are shown in Figure S2 and Table S1.1-1.4 in the Supporting Information. The peaks observed at 284.4 and 285.6 eV are attributed to sp^2 and sp^3 bonds, respectively, while the peak at 288.9 eV is mainly due to the π–π^* transition band.[20] Figure 1a clearly shows that from CNF1000 to CNF1100 to CNF1200 the maximum of the C 1s

X. Mao, Dr. F. Simeon, Prof. G. C. Rutledge, Prof. T. A. Hatton
Department of Chemical Engineering
Massachusetts Institute of Technology
77 Massachusetts Avenue, Cambridge, MA, 02139, USA
E-mail: rutledge@mit.edu; tahatton@mit.edu

DOI: 10.1002/adma.201203045

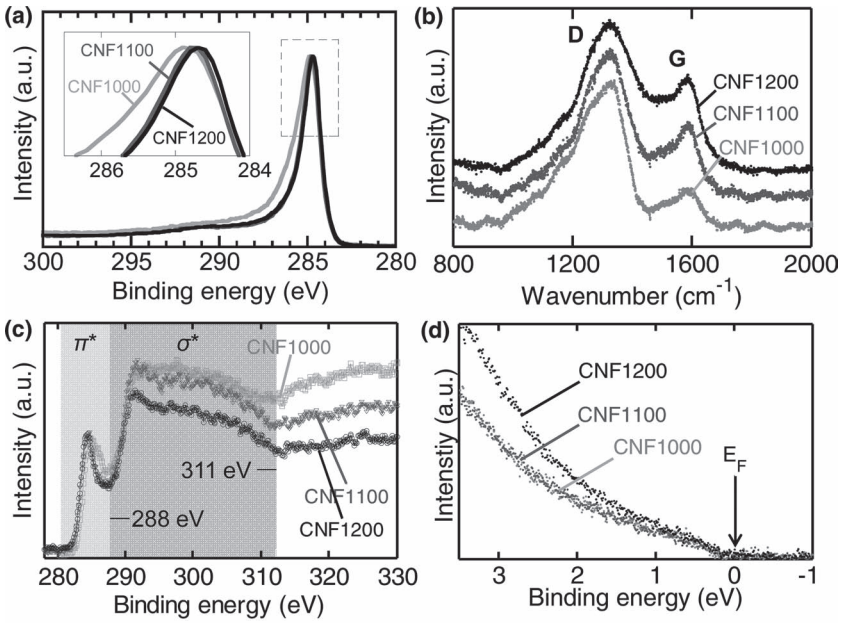

Figure 1. Evidence for control of graphite concentration and DOS for the CNF webs. a) XPS C 1s spectra (the inset is an enlarged dotted rectangle). b) Raman spectra. c) EELS spectra. d) UPS spectra showing the DOS near the Fermi energy.

spectrum is shifted to lower binding energies. This shift indicates that graphite concentration increases with carbonization temperature since the sp^2 bond has a lower binding energy than the sp^3 bond. A broader peak in CNF1000 compared to CNF1100 and CNF1200 also suggests that CNF1000 has higher sp^3 content. In fact the sp^2/sp^3 ratio, calculated from deconvoluted C 1s spectra (Supporting Information, Table S1.4), increases from CNF1000 (1.07 ± 0.01) to CNF1100 (1.17 ± 0.01) to CNF1200 (1.41 ± 0.01). Raman spectra (Figure 1b) show that the R_I-value (the intensity of the D-band at 1330 cm^{-1} divided by that of the G-band at 1590 cm^{-1}) decreases from CNF1000 (3.87) to CNF1100 (2.04) to CNF1200 (1.75). A lower R_I-value indicates higher sp^2 content for carbonaceous materials.[21] Therefore the Raman analyses confirm that higher temperature treatment gives rise to higher graphite concentration. The size of graphite domains (L_c) can be estimated from the X-ray diffraction (XRD) patterns of the CNF webs (Supporting Information, Figure S5) using the Scherrer formula.[14] L_c for CNF1000, CNF1100, and CNF1200 was estimated to be 0.7, 0.8, and 1.0 nm, respectively, suggesting that slightly larger nanometric graphite domains are indeed generated at higher carbonization temperature. Furthermore, electron energy loss spectra (EELS) of the CNF webs (Figure 1c) were used to estimate the ratios of π orbitals to σ orbitals. The peak from 280 to 288 eV and the band from 288 to 311 eV are due to excitation of electrons to the π^* and σ^* states, respectively.[22] The ratio of the integrated areas under these two energy windows approximates the π/σ ratio, which is 1/3 and 0/4 for purely sp^2 and sp^3 bonded carbon, respectively. A higher π/σ ratio implies a higher graphite concentration. The π/σ ratios increased from 0.1097 to 0.1153 to 0.1383 for CNF1000, CNF1100 and CNF1200, respectively, indicating that the number of sp^2 bonds increases with carbonization temperature. Data processing for the XPS C 1s, Raman, and EELS spectra are presented in Section SI3.

We further investigate whether a higher concentration of nanosized graphite domains indeed generates a higher DOS in the CNF webs. Information on the DOS of semimetal carbonaceous materials can be inferred from their electronic conductivity.[1c,23] A higher DOS, which can provide effective overlap of the wave functions of the π electrons of individual sp^2 crystallites, results in a higher conductivity. The measured conductivity of CNF1000, CNF1100 and CNF1200 is 4.32 ± 0.72, 7.88 ± 1.41, and 23.37 ± 1.05 S cm^{-1}, respectively. A positive correlation can be clearly seen between the graphite concentration (indicated by the sp^2/sp^3 or π/σ ratio) and conductivity, both increasing with carbonization temperature. He(I) ultraviolet photoemission spectroscopy (UPS) can be used to probe directly the DOS of carbonaceous materials since the normalized intensity of the spectrum depends on the DOS of the materials investigated.[24] The full UPS spectra normalized by the total integrated intensity (Supporting Information, Figure S6) show that the CNF webs exhibited valence structures that are consistent with graphite valence bands: the intensity from 0 to 3 eV is attributed to pπ-bands, the intensity from 3 to 12 eV arises from pσ-bands, and the intensity at higher binding energies from 12 to 15 eV is the result of an s-like σ-band.[25] For electron-transfer kinetics, the DOS near the Fermi level (E_F = 0 eV) from 0 to 3 eV is important. Figure 1d shows the details of the normalized UPS spectra near E_F for the CNF webs, suggesting that the DOS near E_F for CNF1200 is significantly higher than those for CNF1100 and CNF1000 whereas the DOS of the latter two are almost indistinguishable. This is consistent with the finding that the conductivities of CNF1000 and CNF1100 are similar, whereas the conductivity of CNF1200 is much higher.

The surface nanostructures of the carbonized fibers were probed by high-resolution transmission electron microscopy (HR-TEM) and atomic force microscopy (AFM) The resulting images of the CNF surfaces are shown in **Figure 2**. It has been suggested that, for carbonaceous materials, the ordered structures with stacked parallel stripes seen in the TEM images (Figure 2a, black rectangles) correspond to graphite domains composed of graphene sheets perpendicular to the surface.[4,26] CNF1000 contains very few such structures; in contrast, CNF1100 appears to have ribbon-like graphite domains (the area between the gray lines) and CNF1200 shows extended and interconnected graphite domains. The Fourier transforms for CNF1100 and CNF1200 show a ring-like structure, corresponding to the evenly spaced stripes (i.e., the edges of stacked graphene sheets) with relatively random orientation, whereas the Fourier transform for CNF1000 exhibits no rings at all, indicating that very few ordered structures exist. Moreover, AFM amplitude images (Figure 2b) reveal that CNF1100 and CNF1200 contain more ribbon-like structures than CNF1000, which we attribute to the presence of graphite domains. The TEM and AFM results suggest that more graphite domains

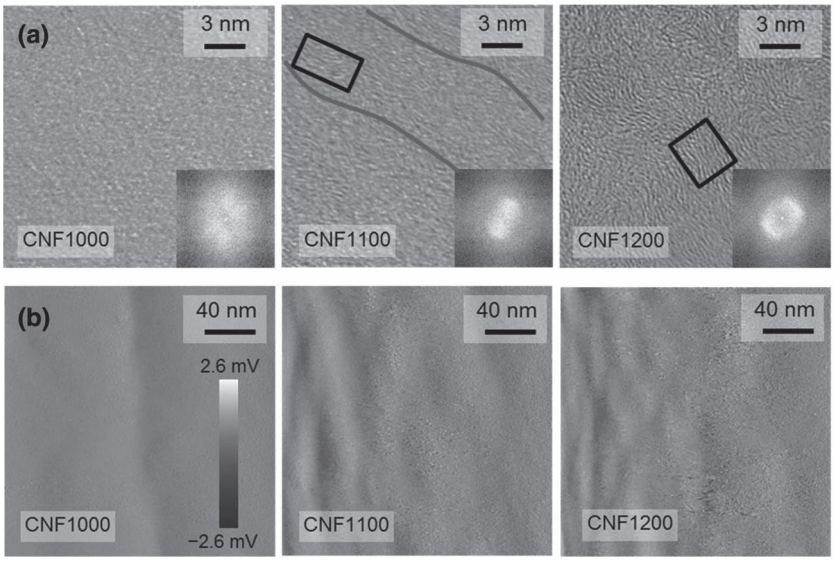

Figure 2. CNF surface nanostructures. a) HR-TEM images (the insets are Fourier transforms). b) AFM amplitude images.

are generated on the CNF surfaces at higher carbonization temperature.

Next we examine the electrochemical activity and biosensitivity of the CNF webs with differing DOS; the results are summarized in **Figure 3**. McCreery[1c] has suggested that redox species can be classified into four general categories, depending on their kinetic sensitivity to surface conditions: i) outer-sphere, ii) oxide-sensitive, iii) adsorption-assisted, and iv) surface-sensitive but not affected by oxide or adsorption. To investigate the electrochemical activity of the CNF webs, we selected four redox couples, $Ru(NH_3)_6^{3+/2+}$, $Fe^{3+/2+}$, dopamine (DA), and $Fe(CN)_6^{3-/4-}$, representing each of the four categories. The apparent electron transfer rates (k^0_{app}) were obtained by cyclic voltammetric analysis using the Nicholson model[27] (see Supporting Information, Section SI7), which is a typical method to evaluate k^0_{app} on carbon-based electrodes.[28] $Ru(NH_3)_6^{3+/2+}$ is an ideal outer-sphere system with kinetics that depend only on the DOS of the electrode.[1c,29] It serves as a benchmark system with which to compare different electrode materials. Values of k^0_{app} on our CNF webs are summarized in Figure 3a and compared with previously reported values of k^0_{app} for other carbon materials.[1c] For the CNF webs, k^0_{app} increases from CNF1000 (0.0055 cm s^{-1}) to CNF1100 (0.0078 cm s^{-1}) to CNF1200 (0.5 cm s^{-1}), which is attributed to the different DOS of the CNF webs. The electron-transfer rate quantified by k^0_{app} increases only slightly from CNF1000 to CNF1100 (1.4-fold), but increases significantly with CNF1200 (91.9-fold), consistent with the conductivity and UPS results on their DOS. k^0_{app} on CNF1000 is slightly higher than that obtained on the basal plane of highly ordered pyrolytic graphite (HOPG),[30] possibly due to the existence of exposed edge-plane sites (even though not at a high density) on the CNF1000 surface. k^0_{app} on CNF1200 is the highest value among the different carbon surfaces, and the ΔE_p of 58 mV (i.e, k^0_{app} = 0.5 cm s^{-1}) is consistent with the theoretical prediction of a kinetically reversible system.[27] Glassy carbon (GC) has a surface that is rich in edge sites; it usually serves as a reference edge-plane surface.[30] However, the GC surface is susceptible to adventitious contamination by impurities, often decreasing k^0_{app}. k^0_{app} of $Ru(NH_3)_6^{3+/2+}$ on GC after different cleaning processes has been investigated,[29,31] and only ultraclean polish[29] results in reversible behavior. In contrast, CNF1200 exhibits reversible electron transfer without any cleaning procedure. In fact, CNF1200 outperforms most carbon surfaces listed in Figure 3a, probably due to its very high edge-plane site density and DOS. Even though boron-doped nanocrystalline diamond and electron-cyclotron-resonance carbon film also exhibit reversible behavior, CNF1200 has many other advantages for electrocatalysis such as its high porosity and free-standing nature.

We further investigated the inner-sphere systems, $Fe^{3+/2+}$, DA, and $Fe(CN)_6^{3-/4-}$, that have varying surface sensitivity. The DOS of the electrode, however, still plays an important role in its electron-transfer kinetics. The k^0_{app} values for the three systems are summarized in Figure 3b. Firstly, the electrode kinetics of $Fe^{3+/2+}$ are sensitive to surface oxide, with a higher O/C ratio resulting in a faster electron transfer.[32] For the CNF webs, treatment at higher temperature removes more heteroatoms and decreases the O/C ratio. However, edge-plane sites, which are generated more easily at higher carbonization temperature, are prone to reactions with oxygen and water, and therefore increase the O/C ratio. The O/C ratios determined from XPS survey scans for CNF1000, CNF1100, and CNF1200 are 0.0276 ± 0.0012, 0.0154 ± 0.0018, and 0.0294 ± 0.0017, respectively (see Supporting Information, Section SI8). The ratio neither increases nor decreases monotonically, indicating the competing effects of carbonization degree and edge-plane sites density. Surprisingly, k^0_{app} for $Fe^{3+/2+}$ still increases monotonically from CNF1000 (0.0003 cm s^{-1}) to CNF1100 (0.0005 cm s^{-1}) to CNF1200 (0.0015 cm s^{-1}). Compared with CNF1000, a low O/C ratio on CNF1100 should lead to a decrease in k^0_{app}. A slight increase of k^0_{app} on CNF1100, relative to that on CNF1000, reflects the tradeoff between the effects of DOS and surface oxide content. More importantly, while CNF1000 and CNF1200 have nearly the same O/C ratio, k^0_{app} on CNF1200 is almost four times that on CNF1000, which is attributed to the high DOS of CNF1200. Secondly, DA requires adsorption to the carbon surface for effective electron transfer.[33] k^0_{app} of DA on CNF1000, CNF1100, and CNF1200 increases from 1.9×10^{-4} to 7.0×10^{-4} to 2.9×10^{-3} cm s^{-1}. The high polarizability of graphite results in strong induced dipoles; therefore a higher concentration of nanosized graphite should lead to more effective adsorption. It is also possible that adsorption is stronger with a higher edge-plane site density, which provides strong dipole-dipole and electrostatic interactions with DA.[34] It is plausible that a synergy between adsorption force and DOS leads to an increasing k^0_{app} for DA from CNF1000 to CNF1100 to CNF1200. Lastly, the kinetics for $Fe(CN)_6^{3-/4-}$ are neither oxide-sensitive nor adsorption-assisted, but possibly influenced by edge-plane site density.[35] From CNF1000

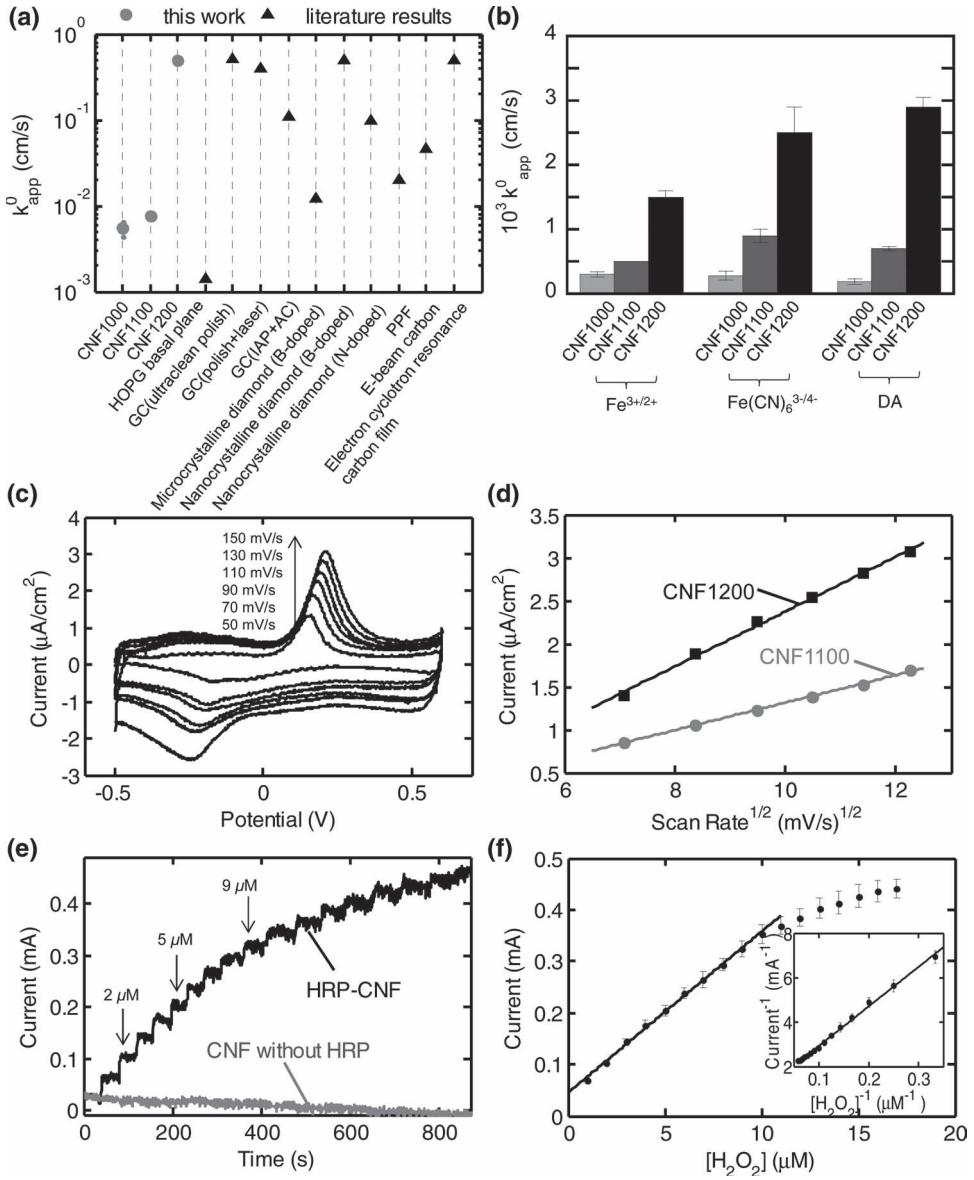

Figure 3. Electrochemical activity and biosensitivity of the CNF webs. a) Comparison of k^0_{app} with literature results[1c] for $Ru(NH_3)_6^{3+/2+}$. b) k^0_{app} for $Fe^{3+/2+}$, DA, and $Fe(CN)_6^{3-/4-}$. c) Background-subtracted cyclic voltammograms of 100 μM Cyt *c* on CNF1200 with increasing scan rates. d) Anodic peak current versus scan rate$^{1/2}$ (R^2 = 0.9985 for CNF1200, R^2 = 0.9989 for CNF1100). e) Amperometric responses of HRP-CNF1200 and pristine CNF1200 at –0.35 V upon additions of H_2O_2 to pH 7.0 phosphate buffer solution with stirring. f) The calibration curve for HRP-CNF1200 (R^2 = 0.9986). The inset shows the Lineweaver–Burk plot (R^2 = 0.9983).

to CNF1100 to CNF1200, k^0_{app} for $Fe(CN)_6^{3-/4-}$ increases from 2.8×10^{-4} to 9.0×10^{-4} to 2.5×10^{-3} cm s^{-1}, probably due to the differences in edge-plane site density. In conclusion, our kinetic studies on the three inner-sphere systems show that the CNF webs exhibit controlled electrochemical activity for all species despite their differing kinetic sensitivities.

Since the DET processes for many redox enzymes are highly dependent upon the DOS of the electrodes,[6] we investigated the enzyme DET efficiencies on the CNF webs with different DOS. Cytochrome *c* (Cyt *c*) is one of the best-studied DET-type enzymes.[4,36] We first tested the biosensitivities of a GC electrode and a graphitized carbon microfiber electrode (Toray carbon paper) toward Cyt *c*. The voltammograms were exactly the same with and without Cyt *c* for both GC and Toray carbon paper, indicating that the DET efficiencies are very low. In contrast, CNF1200 exhibited remarkable bioelectrocatalytic activity for Cyt *c*; we observed quasi-reversible, stable, diffusion-controlled kinetics at the CNF1200 surface. Figure 3c shows a series of background-subtracted cyclic voltammograms (CV) for Cyt *c* obtained on CNF1200 at different scan rates from 50 to 150 mV s^{-1}. A well-defined voltammetric response, characteristic of a quasi-reversible, diffusion-controlled redox reaction, was observed in the potential range of –0.5 to 0.5 V. The observed cathodic peak currents from –0.17 to –0.26 V and the anodic peak currents from 0.14 to 0.22 V at varying scan rates are attributed to the DET-type bioelectrocatalysis current for

Cyt *c*.[4,36a,37] The voltammetric response was observed immediately upon introducing Cyt *c* solution into the electrochemical cell, and there was no deviation from the initial response after 100 sequential scans. A similar well-defined and stable voltammetric response for Cyt *c* was also observed on CNF1100 (Supporting Information, Figure S14). The linearity between the anodic peak currents and the square root of the scan rate (Figure 3d) confirms a quasi-reversible, diffusion-controlled kinetic behavior of Cyt *c* on both CNF1200 and CNF1100. Figure 3d also shows that the magnitudes of the catalytic anodic peak current on CNF1200 are amplified compared with those on CNF1100, suggesting that the DET efficiency is higher on CNF1200 than on CNF1100. The magnitudes of these catalytic currents are comparable to the values on nanostructured carbon films.[4] Moreover, the peak-to-peak separation values (ΔE_p) for Cyt *c* on CNF1200 at different scan rates are significantly reduced compared with the ΔE_p values obtained on CNF1100 (Supporting Information, Figure S15), indicating a much faster electron transfer process on CNF1200. The k^0_{app} values, calculated from ΔE_{p-} via the Nicholson method, are almost 10 times higher on CNF1200 than on CNF1100 (Supporting Information, Figure S16). k^0_{app} for CNF1200 obtained at a low scan rate of 50 mV s^{-1} is 1.3×10^{-4} cm s^{-1}, which is in accordance with the rate constant reported for other bare electrodes without using redox mediators.[38] In contrast to CNF1100 and CNF1200, CNF1000 showed a featureless cyclic voltammogram in the presence of Cyt *c* (Supporting Information, Figure S17), indicating a low DET efficiency.

With the goal of developing a potential biosensing platform, we immobilized another DET-type enzyme, horseradish peroxidase (HRP), onto the CNF webs to test if the enzyme can exhibit its typical catalytic activity toward the reduction of H_2O_2. CNF1000 and CNF1100 immobilized with HRP showed no catalytic response. In contrast, the typical voltammetric response of HRP to increasing concentration of H_2O_2[39] was detected when the enzyme was immobilized on CNF1200 (Supporting Information, Figure S18), revealing that CNF1200 has a high DET efficiency with HRP. To further illustrate the relationship between the electrocatalytic reduction current and the concentration of H_2O_2, the steady-state amperometric response of HRP-CNF1200 to successive additions of H_2O_2 up to 17 μM was recorded at a fixed potential of –0.35 V (Figure 3e). The current response increased with H_2O_2 concentration. Prior to HRP immobilization, the CNF web exhibited a negligible amperometric response upon addition of H_2O_2. HRP-CNF1200 reached 95% of the steady-state current within 2 s, suggesting a rapid electrocatalytic response. The response to the concentration of H_2O_2 was linear over the range from 1 to 10 μM (Figure 3f). The detection limit was estimated to be 1.3 μM based on 3σ (where σ is the standard deviation of the blank solution, number of experiments = 10), and the sensitivity was 31200 μA mM^{-1}. Figure 3f also shows saturation of the current, which is consistent with Michaelis–Menten kinetics. The apparent Michaelis–Menten constant (K_m), calculated from the electrochemical version of the Lineweaver–Burk plot (Figure 3f inset, also see Section SI10.2), was 15.3 μM. A lower K_m indicates a higher enzymatic affinity for the substrate. Compared with other mediator-free DET-type H_2O_2 biosensors (Supporting Information, Table S9), HRP-CNF1200 has a comparable detection limit, a higher sensitivity and a smaller K_m. Moreover, HRP-CNF1200 showed satisfactory selectivity, reproducibility, and stability (Supporting Information, Section SI10.4).

In conclusion, we have demonstrated a new strategy to develop a sensing platform with exceptional electrochemical activity and biosensitivity. The DOS of the CNF webs can be easily varied by controlling their nanosized graphite concentration through manipulation of carbonization conditions. The CNF webs showed controlled kinetic behavior for four different types of redox systems and adjustable DET efficiencies for Cyt *c*. HRP-modified CNF webs with a high DOS exhibited the desired electrocatalytic response. Our findings indicate the utility of these materials in molecular and biomolecular electrochemistry, and point towards novel applications for carbonized electrospun nanofiber webs in sensing and electrocatalysis.

Experimental Section

PAN fibers were electrospun from 10 wt% solutions in dimethylformamide (DMF) using a parallel-plate apparatus, as described elsewhere.[40] The applied potential, solution flow rate, and spin distance were 30 kV, 0.02 mL min^{-1}, and 30 cm, respectively (see Supporting Information, Section SI1.2). The resulting webs were stabilized in air at 270 °C for 1 h and then carbonized under nitrogen at 1000–1200 °C for 1 h (tube furnace, MTI, GSL-1800S60). The heating rate was 5 °C min^{-1} from room temperature to 270 °C and 3 °C min^{-1} from 270 to 1000–1200 °C. A pressure of 176 g m^{-2} was applied to the webs using molybdenum plates. Characterization methods of the CNF webs are described in Section SI1.3 in the Supporting Information. Electrochemical experiments were performed using an AutoLab PGSTAT30 potentiostat. The working electrode was the CNF web. A platinum wire and an Ag/AgCl electrode (BASi) were the auxiliary and reference electrodes, respectively. For the Cyt *c* study, epoxy resin was used to mask off part of the electrode to control the extent of the electrode that comes in contact with the electrolyte solution. The amperometric response was normalized with respect to the surface area. For the HRP immobilization, HRP (1×10^{-3} M)/tris-(hydroxymethyl)-aminomethane (TRIS) (1×10^{-2} M) solution (50 μL) was drop-cast to the CNF web.

Supporting Information

Supporting Information is available from the Wiley Online Library or from the author.

Acknowledgements

This work was supported by U.S. Department of Energy. We thank Prof. Ying Yang from Tsinghua University for the helpful discussions on the synthesis of electrospun CNF webs.

Received: July 26, 2012
Revised: November 3, 2012
Published online: December 19, 2012

[1] a) J. M. Saveant, *Chem. Rev.* **2008**, *108*, 2111; b) J. M. Savéant, *Elements of Molecular and Biomolecular Electrochemistry*; Wiley, New York**2006**; c) R. L. McCreery, *Chem. Rev.* **2008**, *108*, 2646.

[2] a) I. Dumitrescu, P. R. Unwin, J. V. Macpherson, *Chem. Commun.* **2009**, 6886; b) M. Pumera, *Chem. Soc. Rev.* **2010**, *39*, 4146.

[3] a) A. Ambrosi, T. Sasaki, M. Pumera, *Chem. Asian J.* **2010**, *5*, 266; b) E. C. Landis, K. L. Klein, A. Liao, E. Pop, D. K. Hensley, A. V. Melechko, R. J. Hamers, *Chem. Mater.* **2010**, *22*, 2357.
[4] A. Ueda, D. Kato, R. Kurita, T. Kamata, H. Inokuchi, S. Umemura, S. Hirono, O. Niwa, *J. Am. Chem. Soc.* **2011**, *133*, 4840.
[5] a) W. J. Royea, T. W. Hamann, B. S. Brunschwig, N. S. Lewis, *J. Phys. Chem. B* **2006**, *110*, 19433; b) R. Parsons, *Surf. Sci.* **1964**, *2*, 418.
[6] C. Leger, P. Bertrand, *Chem. Rev.* **2008**, *108*, 2379.
[7] L. Stoica, R. Ludwig, D. Haltrich, L. Gorton, *Anal. Chem.* **2006**, *78*, 393.
[8] M. Pita, E. Katz, *J. Am. Chem. Soc.* **2008**, *130*, 36.
[9] K. A. Vincent, X. Li, C. F. Blanford, N. A. Belsey, J. H. Weiner, F. A. Armstrong, *Nat. Chem. Biol.* **2007**, *3*, 760.
[10] J. A. Cracknell, K. A. Vincent, F. A. Armstrong, *Chem. Rev.* **2008**, *108*, 2439.
[11] Y. Dzenis, *Science* **2004**, *304*, 1917.
[12] M. Inagaki, Y. Yang, F. Y. Kang, *Adv. Mater.* **2012**, *24*, 2547.
[13] a) C. Kim, B. T. N. Ngoc, K. S. Yang, M. Kojima, Y. A. Kim, Y. J. Kim, M. Endo, S. C. Yang, *Adv. Mater.* **2007**, *19*, 2341; b) B. H. Kim, K. S. Yang, H. G. Woo, *Electrochem. Commun.* **2011**, *13*, 1042.
[14] C. Kim, K. S. Yang, M. Kojima, K. Yoshida, Y. J. Kim, Y. A. Kim, M. Endo, *Adv. Funct. Mater.* **2006**, *16*, 2393
[15] M. Y. Li, G. Y. Han, B. S. Yang, *Electrochem. Commun.* **2008**, *10*, 880.
[16] a) J. S. Huang, D. W. Wang, H. Q. Hou, T. Y. You, *Adv. Funct. Mater.* **2008**, *18*, 441; b) Y. Liu, D. W. Wang, L. Xu, H. Q. Hou, T. Y. You, *Biosens. Bioelectron.* **2011**, *26*, 4585.
[17] a) Y. Yang, A. Centrone, L. Chen, F. Simeon, T. A. Hatton, G. C. Rutledge, *Carbon* **2011**, *49*, 3395; b) Y. Yang, F. Simeon, T. A. Hatton, G. C. Rutledge, *J. Appl. Polym. Sci.* **2012**, *124*, 3861.
[18] K. J. Koivusaari, T. T. Rantala, S. Leppavuori, *Diamond Relat. Mater.* **2000**, *9*, 736.
[19] A. Greiner, J. H. Wendorff, *Angew. Chem. Int. Ed.* **2007**, *46*, 5670.
[20] H. Estrade-Szwarckopf, *Carbon* **2004**, *42*, 1713.
[21] M. A. Pimenta, G. Dresselhaus, M. S. Dresselhaus, L. G. Cancado, A. Jorio, R. Saito, *Phys. Chem. Chem. Phys.* **2007**, *9*, 1276.
[22] J. J. Cuomo, J. P. Doyle, J. Bruley, J. C. Liu, *Appl. Phys. Lett.* **1991**, *58*, 466.
[23] K. K. Cline, M. T. McDermott, R. L. McCreery, *J. Phys. Chem.* **1994**, *98*, 5314.
[24] J. D. Wiggins-Camacho, K. J. Stevenson, *J. Phys. Chem. C* **2009**, *113*, 19082.
[25] F. R. McFeely, S. P. Kowalczy, L. Ley, R. G. Cavell, R. A. Pollak, D. A. Shirley, *Phys. Rev. B* **1974**, *9*, 5268.
[26] S. Hirono, S. Umemura, M. Tomita, R. Kaneko, *Appl. Phys. Lett.* **2002**, *80*, 425.
[27] R. Nicholson, *Anal. Chem.* **1965**, *37*, 1351.
[28] W. Li, C. Tan, M. A. Lowe, H. D. Abruna, D. C. Ralph, *ACS Nano* **2011**, *5*, 2264.
[29] S. Ranganathan, T. C. Kuo, R. L. McCreery, *Anal. Chem.* **1999**, *71*, 3574.
[30] K. R. Kneten, R. L. McCreery, *Anal. Chem.* **1992**, *64*, 2518.
[31] a) I. F. Hu, D. H. Karweik, T. Kuwana, *J. Electroanal. Chem.* **1985**, *188*, 59; b) R. J. Rice, N. M. Pontikos, R. L. McCreery, *J. Am. Chem. Soc.* **1990**, *112*, 4617.
[32] P. H. Chen, M. A. Fryling, R. L. McCreery, *Anal. Chem.* **1995**, *67*, 3115.
[33] S. H. DuVall, R. L. McCreery, *J. Am. Chem. Soc.* **2000**, *122*, 6759
[34] M. T. McDermott, K. Kneten, R. L. McCreery, *J. Phys. Chem.* **1992**, *96*, 3124.
[35] C. E. Banks, R. G. Compton, *Analyst* **2006**, *131*, 15
[36] a) S. Haymond, G. T. Babcock, G. M. Swain, *J. Am. Chem. Soc.* **2002**, *124*, 10634; b) S. Alwarappan, R. K. Joshi, M. K. Ram, A. Kumar, *Appl. Phys. Lett.* **2010**, *96*
[37] M. Tominaga, N. Hirata, I. Taniguchi, *Electrochem. Commu.n* **2005**, *7*, 1423.
[38] C. Mu, Q. Zhao, D. S. Xu, Q. K. Zhuang, Y. H. Shao, *J. Phys. Chem. B* **2007**, *111*, 1491.
[39] O. A. de Fuentes, T. Ferri, M. Frasconi, V. Paolini, R. Santucci, *Angew. Chem. Int. Ed.* **2011**, *50*, 3457.
[40] Y. M. Shin, M. M. Hohman, M. P. Brenner, G. C. Rutledge, *Polymer* **2001**, *42*, 9955.